Electronic Supplementary Information

Wrinkle-induced highly conductive channels in graphene on SiO_2/Si substrate

Rui-Song Ma[1, 2] ‡, Jiajun Ma[1, 2] ‡, Jiahao Yan[1, 2], Liangmei Wu[1, 2], Wei Guo[4], Shuai Wang[4], Qing Huan[1, 2], Lihong Bao[1, 2, 3,*], Sokrates T. Pantelides[5, 2], and Hong-Jun Gao[1, 2]

[1]*Institute of Physics, Chinese Academy of Sciences, PO Box 603, Beijing 100190, People's Republic of China*

[2] *University of Chinese Academy of Sciences & CAS Center for Excellence in Topological Quantum Computation, Chinese Academy of Sciences, PO Box 603, Beijing 100190, People's Republic of China*

[3]*Songshan Lake Materials Laboratory, Dongguan, Guangdong 523808, People's Republic of China*

[4]*Key Laboratory of Material Chemistry for Energy Conversion and Storage, Ministry of Education School of Chemistry and Chemical Engineering, Huazhong University of Science and Technology, Wuhan, 430074, People's Republic of China*

[5]*Department of Physics and Astronomy and Department of Electrical Engineering and Computer Science, Vanderbilt University, Nashville, Tennessee 37235, United States*

E-mail: lhbao@iphy.ac.cn

‡ These authors contributed equally to this work.

Spacing-variable four-probe measurement

In the four-probe measurement, probe 1 injects electrical current (*I*1) and probe 4 is grounded (*G*4). Probe 2 and 3 are potential probes which measure the potential difference between them (*V*23=*V*2-*V*3). The measurement configuration is named as *I*1*V*23 and the measured resistance R_{I1V23} is defined as *V*23/*I*1 (in unit Ω).[1]

The four-probe resistivity measurements are intrinsically dependent on geometry and dimensionality, and sensitive to the probe positions.[1] Therefore, the four-probe measurements can be used to characterize the dimensionality of transport behaviors.[2, 3] In this paper, r_{ij} is defined as the probe distance between probe *i* and *j*. Next, the relationship of measured resistance and probe distances for 3D, 2D and 1D case will be introduced in detail.

3D case

On condition that the current entering via probe 1 is I_1, the current density J_1 is given by

$$J_1(r) = \frac{I_1}{2\pi r^2}. \tag{S1}$$

The electric field *E*(r) yielded by J_1 is expressed by

$$E(r) = \rho_{\mathrm{3D}} J_1(r) = \frac{\rho_{\mathrm{3D}} I_1}{2\pi r^2} = -\frac{\mathrm{d}V(r)}{\mathrm{d}r}, \tag{S2}$$

where ρ_{3D} is the resistivity in the 3D case.

Accordingly, potential at probe 2 can be written as

$$0 - V_2 = \int_{r_{12}}^{\infty} \frac{\mathrm{d}V(r)}{\mathrm{d}r}\mathrm{d}r = -\int_{r_{12}}^{\infty} \frac{\rho_{\mathrm{3D}} I_1}{2\pi r^2}\mathrm{d}r = \left.\frac{\rho_{\mathrm{3D}} I_1}{2\pi r}\right|_{r_{12}}^{\infty} = -\frac{\rho_{\mathrm{3D}} I_1}{2\pi r_{12}}. \tag{S3}$$

Similarly, the potential at probe 2 yielded by probe 4 can be written as

$$V_2 = -\int_{r_{12}}^{\infty} \frac{\mathrm{d}V(r)}{\mathrm{d}r}\mathrm{d}r = \int_{r_{12}}^{\infty} \frac{\rho_{3\mathrm{D}} I_4}{2\pi r^2}\mathrm{d}r = -\frac{\rho_{3\mathrm{D}} I_4}{2\pi r}\bigg|_{r_{42}}^{\infty} = \frac{\rho_{3\mathrm{D}} I_4}{2\pi r_{42}}. \tag{S4}$$

Since I_1=-I_4=I, the final expression of the measured potential at probe 2 is

$$V_2 = \frac{\rho_{3\mathrm{D}} I_1}{2\pi r_{12}} + \frac{\rho_{3\mathrm{D}} I_4}{2\pi r_{42}} = \frac{\rho_{3\mathrm{D}} I_1}{2\pi r_{12}} - \frac{\rho_{3\mathrm{D}} I_1}{2\pi r_{42}}. \tag{S5}$$

By the same method, the final expression of the measured potential at probe 3 is

$$V_3 = \frac{\rho_{3\mathrm{D}} I_1}{2\pi r_{13}} + \frac{\rho_{3\mathrm{D}} I_4}{2\pi r_{43}} = \frac{\rho_{3\mathrm{D}} I_1}{2\pi r_{13}} - \frac{\rho_{3\mathrm{D}} I_1}{2\pi r_{43}}. \tag{S6}$$

The potential difference between probe 2 and probe 3 caused by the total diffusing current can be described by

$$V_2 - V_3 = \frac{\rho_{3D} I_1}{2\pi r_{12}} - \frac{\rho_{3D} I_1}{2\pi r_{42}} - \left(\frac{\rho_{3D} I_1}{2\pi r_{13}} - \frac{\rho_{3D} I_1}{2\pi r_{43}}\right) = \frac{\rho_{3D} I_1}{2\pi}\left(\frac{1}{r_{12}} + \frac{1}{r_{43}} - \frac{1}{r_{42}} - \frac{1}{r_{13}}\right). \tag{S7}$$

Therefore, the relationship between the measured resistance V23/I1 and the 3D resistivity is

$$R_{I1V23} = \frac{V_2 - V_3}{I_1} = \frac{\rho_{3D}}{2\pi}\left(\frac{1}{r_{12}} + \frac{1}{r_{43}} - \frac{1}{r_{42}} - \frac{1}{r_{13}}\right). \tag{S8}$$

In the case of collinear configuration as shown in Fig. S2(a), the coordinates of each tip are P1[-3 0], P2[-1 0], P3[x 0] and P4[0 0]. And then

$$R_{I1V23} = \frac{\rho_{3D}}{2\pi}\left(\frac{1}{2} + \frac{1}{\mathrm{abs}(x)} - 1 - \frac{1}{\mathrm{abs}(x+3)}\right). \tag{S9}$$

The expression in the bracket above is named as geometry factor for 3D case, the plot of which is shown in Fig. S2(d).

2D case

On condition that the current entering via probe 1 is I_1 and the sample thickness is t, the current density J_1 is given by

$$J_1(r) = \frac{I_1}{2\pi r t}. \tag{S10}$$

The electric field E(r) yielded by J_1 is expressed by

$$E(r) = \rho_{3\mathrm{D}} J_1(r) = \frac{\rho_{3\mathrm{D}} I_1}{2\pi r t} = \frac{\rho_{2\mathrm{D}} I_1}{2\pi r} = -\frac{\mathrm{d}V(r)}{\mathrm{d}r}, \tag{S11}$$

where $\rho_{2\mathrm{D}}$ is the resistivity in the 2D case.

Accordingly, potential at probe 2 can be written as

$$0 - V_2 = \int_{r_{12}}^{\infty} \frac{\mathrm{d}V(r)}{\mathrm{d}r}\mathrm{d}r = -\int_{r_{12}}^{\infty} \frac{\rho_{2\mathrm{D}} I_1}{2\pi r}\mathrm{d}r = -\frac{\rho_{2\mathrm{D}} I_1}{2\pi}\ln(r)\Big|_{\mathrm{r}_{12}}^{\infty} = \frac{\rho_{2\mathrm{D}} I_1}{2\pi}\ln(r_{12}). \tag{S12}$$

Similarly, the potential at probe 2 yielded by probe 4 can be written as

$$V_2 = -\int_{r_{42}}^{\infty} \frac{\mathrm{d}V(r)}{\mathrm{d}r}\mathrm{d}r = \int_{r_{42}}^{\infty} \frac{\rho_{2\mathrm{D}} I_4}{2\pi r}\mathrm{d}r = \frac{\rho_{2\mathrm{D}} I_4}{2\pi}\ln(r)\Big|_{\mathrm{r}_{42}}^{\infty} = -\frac{\rho_{2\mathrm{D}} I_4}{2\pi}\ln(r_{42}). \tag{S13}$$

Since I_1=-I_4=I, the final expression of the measured potential at probe 2 is

$$V_2 = -\frac{\rho_{2\mathrm{D}} I_1}{2\pi}\ln(r_{12}) - \frac{\rho_{2\mathrm{D}} I_4}{2\pi}\ln(r_{42}) = -\frac{\rho_{2\mathrm{D}} I_1}{2\pi}\ln(r_{12}) + \frac{\rho_{2\mathrm{D}} I_1}{2\pi}\ln(r_{42}). \tag{S14}$$

By the same method, the final expression of the measured potential at probe 3 is

$$V_3 = -\frac{\rho_{2\mathrm{D}} I_1}{2\pi}\ln(r_{13}) - \frac{\rho_{2\mathrm{D}} I_4}{2\pi}\ln(r_{43}) = -\frac{\rho_{2\mathrm{D}} I_1}{2\pi}\ln(r_{13}) + \frac{\rho_{2\mathrm{D}} I_1}{2\pi}\ln(r_{43}). \tag{S15}$$

The potential difference between probe 2 and probe 3 caused by the total diffusing current can be described by

$$\begin{aligned} V_2 - V_3 &= -\frac{\rho_{2\mathrm{D}} I_1}{2\pi}\ln(r_{12}) + \frac{\rho_{2\mathrm{D}} I_1}{2\pi}\ln(r_{42}) - \left(-\frac{\rho_{2\mathrm{D}} I_1}{2\pi}\ln(r_{13}) + \frac{\rho_{2\mathrm{D}} I_1}{2\pi}\ln(r_{43})\right) \\ &= \frac{\rho_{2D} I_1}{2\pi}\left(\ln(\frac{1}{r_{12}}) + \ln(\frac{1}{r_{43}}) - \ln(\frac{1}{r_{42}}) - \ln(\frac{1}{r_{13}})\right) = \frac{\rho_{2D} I_1}{2\pi}\ln(\frac{r_{13} r_{42}}{r_{12} r_{43}}) \end{aligned}. \tag{S16}$$

Therefore, the relationship between the measured resistance V23/I1 and the 2D resistivity is

$$R_{I1V23}=\frac{V_2-V_3}{I_1}=\frac{\rho_{2D}}{2\pi}\ln(\frac{r_{13}r_{42}}{r_{12}r_{43}})\,. \tag{S17}$$

In the case of collinear configuration as shown in Fig. S2(b), the coordinates of each tip are P1[-3 0], P2[-1 0], P3[x 0] and P4[0 0]. And then

$$R_{I1V23}=\frac{\rho_{2D}}{2\pi}\ln(\frac{abs(x+3)}{2\cdot abs(x)})\,. \tag{S18}$$

The expression in the logarithm function on the right is named as geometry factor for 2D case, the plot of which is shown in Fig. S2(e).

1D case

On condition that the current entering via probe 1 is I_1 and the sample cross-section is s, the current density J_1 is given by

$$J_1(r)=\frac{I_1}{2s}\,. \tag{S19}$$

The electric field E(r) yielded by J_1 is expressed by

$$E(r)=\rho_{3\mathrm{D}}J_1(r)=\frac{\rho_{3\mathrm{D}}I_1}{2s}=\frac{\rho_{1\mathrm{D}}I_1}{2}=-\frac{\mathrm{d}V(r)}{\mathrm{d}r}\,, \tag{S20}$$

where $\rho_{1\mathrm{D}}$ is the resistivity in the 1D case.

Accordingly, potential at probe 2 can be written as

$$0-V_2=\int_{r_{12}}^{\infty}\frac{\mathrm{d}V(r)}{\mathrm{d}r}\mathrm{d}r=-\int_{r_{12}}^{\infty}\frac{\rho_{1\mathrm{D}}I_1}{2}\mathrm{d}r=-\frac{\rho_{1\mathrm{D}}I_1}{2}r\Big|_{\mathrm{r}_{12}}^{\infty}=\frac{\rho_{1\mathrm{D}}I_1}{2}r_{12}\,. \tag{S21}$$

Similarly, the potential at probe 2 yielded by probe 4 can be written as

$$V_2=-\int_{r_{42}}^{\infty}\frac{\mathrm{d}V(r)}{\mathrm{d}r}\mathrm{d}r=\int_{r_{42}}^{\infty}\frac{\rho_{1\mathrm{D}}I_4}{2}\mathrm{d}r=\frac{\rho_{1\mathrm{D}}I_4}{2}r\Big|_{\mathrm{r}_{42}}^{\infty}=-\frac{\rho_{1\mathrm{D}}I_4}{2}r_{42}\,. \tag{S22}$$

Since I_1=-I_4=I, the final expression of the measured potential at probe 2 is

$$V_2=-\frac{\rho_{1\mathrm{D}}I_1}{2}r_{12}-\frac{\rho_{1\mathrm{D}}I_4}{2}r_{42}=-\frac{\rho_{1\mathrm{D}}I_1}{2}r_{12}+\frac{\rho_{1\mathrm{D}}I_1}{2}r_{42}\,. \tag{S23}$$

By the same method, the final expression of the measured potential at probe 3 is

$$V_3 = -\frac{\rho_{1\mathrm{D}} I_1}{2} r_{13} - \frac{\rho_{1\mathrm{D}} I_4}{2} r_{43} = -\frac{\rho_{1\mathrm{D}} I_1}{2} r_{13} + \frac{\rho_{1\mathrm{D}} I_1}{2} r_{43}. \qquad \text{(S24)}$$

The potential difference between probe 2 and probe 3 caused by the total diffusing current can be described by

$$\begin{aligned} V_2 - V_3 &= -\frac{\rho_{1\mathrm{D}} I_1}{2} r_{12} + \frac{\rho_{1\mathrm{D}} I_1}{2} r_{42} - (-\frac{\rho_{1\mathrm{D}} I_1}{2} r_{13} + \frac{\rho_{1\mathrm{D}} I_1}{2} r_{43} \\ &= \frac{\rho_{1D} I_1}{2} (-r_{12} - r_{43} + r_{42} + r_{13} \end{aligned}. \qquad \text{(S25)}$$

Therefore, the relationship between the measured resistance V23/I1 and the 2D resistivity is

$$R_{I1V23} = \frac{V_2 - V_3}{I_1} = \frac{\rho_{1D}}{2} (-r_{12} - r_{43} + r_{42} + r_{13} \;. \qquad \text{(S26)}$$

In the case of collinear configuration as shown in Fig. S2(c), the coordinates of each tip are P1[-3 0], P2[-1 0], P3[*x* 0] and P4[0 0]. And then

$$\begin{aligned} R_{I1V23} &= \frac{\rho_{1D} I_1}{2} (-2 - abs(x) + 1 + abs(x+3)) \\ &= \frac{\rho_{1D} I_1}{2} (-1 + abs(3+x) - abs(x)) \end{aligned}. \qquad \text{(S27)}$$

The expression in the brackets on the right is named as geometry factor for 2D case, the plot of which is shown in Fig. S2(f).

Traditional four-probe measurements in 2D case

As for the 2D case, if the probe distances are much smaller than the lateral dimension of sample, the sheet resistance $R_\square$ (in unit $\Omega/\square$) of the measured 2D sample can be calculated from R_{I1V23} by

$$R_{\square} = \frac{2\pi}{\ln(\frac{r_{13}r_{42}}{r_{12}r_{43}})} R_{I1V23} \quad , \tag{S28}$$

where r_{ij} (=r_{ji}) is defined as the distance between probe *i* and probe *j*.

In the collinear case where the four probes are placed in a line with equal spacing (r_{12}=r_{23}=r_{34}), the $R_{\square}$ can be written as

$$R_{\square} = \frac{\pi}{\ln 2} R_{I1V23} . \tag{S29}$$

As for the square case where the four probes form a square with equal spacing (r_{12}=r_{23}=r_{34}=r_{41}=$r_{13}/\sqrt{2}$= $r_{24}/\sqrt{2}$), the $R_{\square}$ can be written as

$$R_{\square} = \frac{2\pi}{\ln 2} R_{I1V23} . \tag{S30}$$

Resistor network simulation

In order to estimate the conductivity solely within the wrinkled area, we used resistor network simulation to simulate the four-probe collinear measurements along graphene wrinkles, as shown in Fig. S3. Therein, green and light blue resistors represent the 4 μm × 4 μm area for graphene wrinkle and pristine graphene, respectively. By the way, the setting of 4 μm is based on the averaged width of graphene wrinkle in this paper. The four probes are placed with equal spacing of 60 μm according to the experimental setups.

In a network composed of linear and bilateral resistors, the potential distribution is merely determined by the relative resistance or conductance with constant current source and fixed contacts applied. For example, under constant current, the potential drop caused by resistors with 1 Ω, 2 Ω and 3 Ω in series is the same as that caused by

2 Ω, 4 Ω and 6 Ω resistors. That is to say, the resistance ratio of wrinkle (R_w, green) and monolayer (R_m, light blue) resistors result in the potential profile in the four-probe case. In other words, $\sigma\square_{\text{inside-w}}$ (the conductivity inside the wrinkle) and $\sigma\square_{m}$ (the conductivity of pristine monolayer graphene, 1S/□ with R_m equal to 1 Ω) determines the potential distribution with a constant current injection. For convenience, the current injected by probe 1 and R_m are set to be 1 A and 1 Ω, respectively. The resistance of R_w ranges from 1 Ω to $1E^{-4}$ Ω with 100 points selected and for each R_w setting, the calculated conductivity along the wrinkle in the four-probe measurements ($\sigma\square_{\text{along-w}}$) can be obtained from the potential distribution. Accordingly, at each set of R_w, $\sigma\square_{\text{inside-w}}/\sigma\square_{m}$ and $\sigma\square_{\text{along-w}}/\sigma\square_{m}$ are calculated, which is shown in Fig. 4(b) in the main text. For the experimental results, since $\sigma\square_{\text{along-w}}$ and $\sigma\square_{m}$ can be directly obtained from the four-probe measurements, $\sigma\square_{\text{inside-w}}/\sigma\square_{m}$ or $\sigma\square_{\text{inside-w}}$ can be estimated based on the ratio relationship shown in Fig. 4(b).

Estimation of strain distribution by the vector decomposition method

In order to figure out the high conductivity of graphene wrinkle in this paper, Raman characterizations are performed on wrinkled region and monolayer areas near the wrinkle as shown in Fig. 5(a). Figs. 5(b) and (c) show the Raman mapping of 2D and G peak positions of the wrinkled area in (a), respectively. The wrinkled features are clearly shown in the Raman mapping image, especially in the G mode.

By the vector decomposition method introduced by Lee *et al*, the strain can be disentangled from the doping according to the peak positions of Raman 2D (ω_{2D}) and

G (ω_G) modes.[4, 5] In this method, hole doping and randomly uniaxial strain are assumed for graphene on SiO_2/Si substrate. Two vectors showing the changes in G and 2D Raman shift are defined by $\Delta\omega_{2D}$=ω_{2D}-2678 cm^{-1} and $\Delta\omega_G$=ω_G-1587 cm^{-1}, in which 2668 and 1587 cm^{-1} are averaged reference values for the flat region far away from the wrinkled area in this paper (the same as Ref. 5). For the randomly uniaxial strain and hole doping, strain variation ($\Delta\varepsilon$, in %) and doping level (Δn, in $10^{12}/cm^{-2}$) follow the linear relationship: $\Delta\omega_G$ / $\Delta\varepsilon$ (%) = -23.5, $(\Delta\omega_{2D} / \Delta\omega_G)_{\varepsilon,\ n=0}$ = 2.2, $\Delta\omega_g$ / Δn= 1 and $(\Delta\omega_{2D} / \Delta\omega_G)_{n,\ \varepsilon=0}$ = 0.7. Accordingly, the two vectors ($\Delta\omega_{2D}$, $\Delta\omega_G$) can be calculated by,[4, 5]

$$\begin{cases} \Delta\omega_{2D} = -\Delta\varepsilon \bullet 51.7 + \Delta n \bullet 0.7 \\ \Delta\omega_G = -\Delta\varepsilon \bullet 23.5 + \Delta n \end{cases} . \tag{S31}$$

Fig. S7 shows correlation plots of the G and 2D peak positions, based on the Raman characterization in Figs. 5(b-c). The doping vector line with a slope of 0.7 (in blue) and strain vector line with a slope of 2.2 (in red) intersect at point (1587, 2678), which is the averaged peak positions in flat area. The G-2D coordinate space is divided into four quadrants, saying Q1–Q4, by the strain and doping vectors. For any experimental point in Fig. S7, a combination of compressive (tensile) strain and p-doping can be extracted by Equation S31. Q2 and Q3 regions are not allowed because both of n- and p- doping should lead to increasing in ω_G.[4, 6] In our case, most of the experimental points are located in the forbidden Q2 and Q3 regions, which can be attributed to the affection by strain.[4] Based on the vector decomposition method, the strain distribution can be extracted, as shown in Fig. 5(d). As can be seen, the wrinkled regions show compressive strain while the monolayer regions near the wrinkle present tensile strain, so the strain polarity is reversed in boundary of the wrinkle. Therefore, large strain gradients are mainly distributed in the boundary regions with larger curvatures, as verified in Fig. 5(e). Based on the same method, strain distributions of wrinkle-2 can be obtained as shown in Fig. S8.

References

1. I. Miccoli, F. Edler, H. Pfnur and C. Tegenkamp, *J. Phys. Condens. Matter*, 2015, **27**, 223201.
2. S. B. Kjeldby, O. M. Evenstad, S. P. Cooil and J. W. Wells, *J. Phys. Condens. Matter*, 2017, **29**, 394008.
3. C. Durand, X. G. Zhang, S. M. Hus, C. Ma, M. A. McGuire, Y. Xu, H. Cao, I. Miotkowski, Y. P. Chen and A.-P. Li, *Nano lett.*, 2016, **16**, 2213-2220.
4. J. E. Lee, G. Ahn, J. Shim, Y. S. Lee and S. Ryu, *Nat. Commun.*, 2012, **3**, 1024.
5. T. Hallam, A. Shakouri, E. Poliani, A. P. Rooney, I. Ivanov, A. Potie, H. K. Taylor, M. Bonn, D. Turchinovich, S. J. Haigh, J. Maultzsch and G. S. Duesberg, *Nano lett.*, 2015, **15**, 857-863.
6. A. Das, S. Pisana, B. Chakraborty, S. Piscanec, S. K. Saha, U. V. Waghmare, K. S. Novoselov, H. R. Krishnamurthy, A. K. Geim, A. C. Ferrari and A. K. Sood, *Nat. Nanotechnol.*, 2008, **3**, 210.

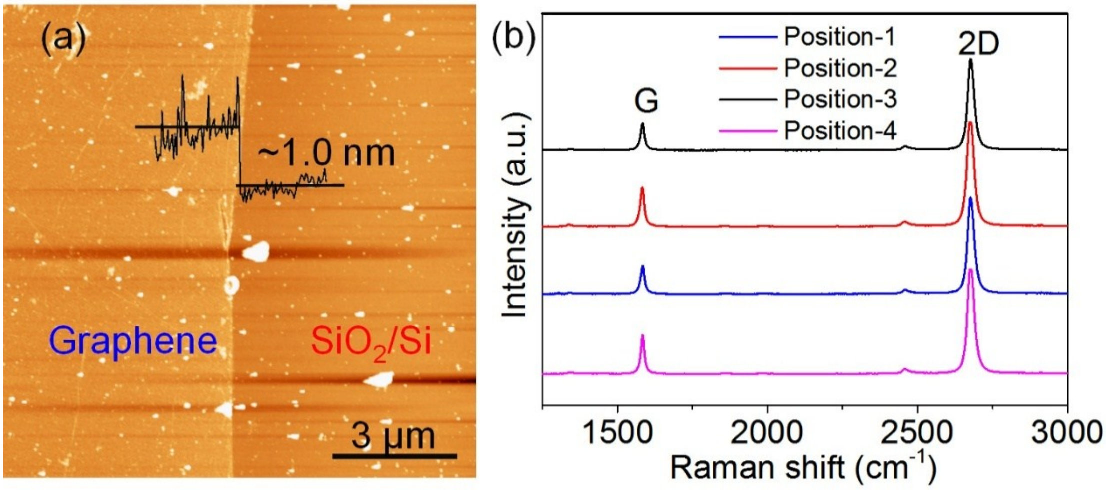

Fig. S1 AFM and Raman characterization of the monolayer graphene region. (a) AFM height image of the graphene edge area on Si/SiO_2 substrate. The inset line profile reveals the thickness of the monolayer graphene area is ~1.0 nm. (b) Raman spectra collected on four random positions on monolayer area. The spectra are offset vertically for clarity. The relative intensity ratio of 2D and G peaks (>2:1) confirms the monolayer nature of the graphene area near the graphene wrinkle. In addition, the absence of the D peak indicates that no detectable defects are found in the transferred graphene sample on the SiO_2/Si substrate.

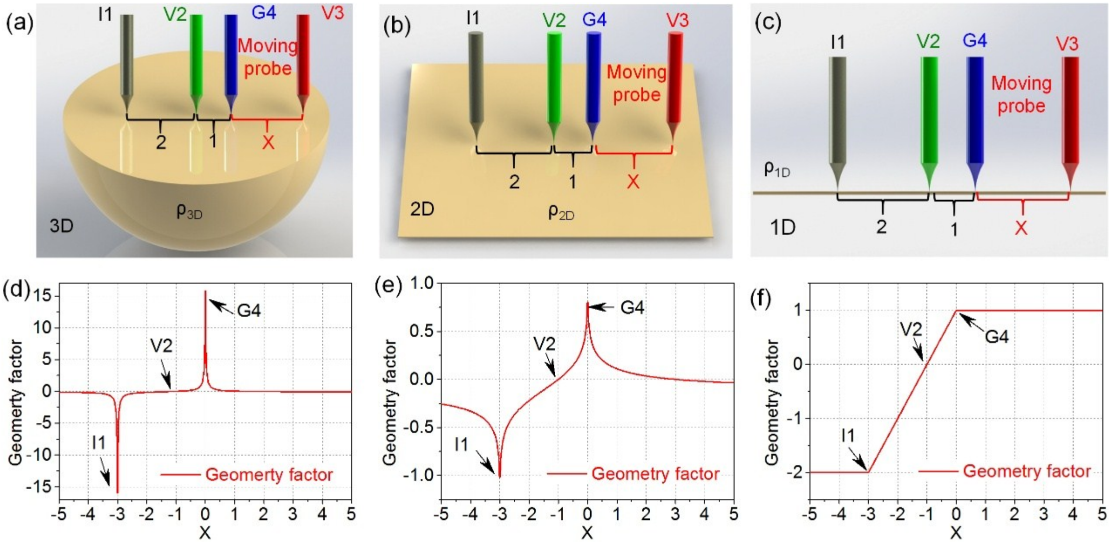

Fig. S2. Four-probe collinear measurements on materials from 3D down to 1D with a moving probe. (a-c) Schematics of four-probe collinear measurements on materials from 3D down to 1D, respectively. The four probes are arranged in a collinear arrangement. Probe 1 (I1) injects the current to the materials and probe 4 (G4) is grounded. Probe 2 and 3 are used to measure the potential distribution on the material surface (V2 and V3). The distance between probe 1 and 2 is fixed to 2 (a.u.) while the distance between probe 4 and 2 is fixed to 1 (a.u.). Probe 3 is a moving probe and the distance between probe 4 and 3 is x (a.u.). (d-f) Geometry factor variations in the four-probe collinear measurements on materials from 3D down to 1D, respectively. The black arrows indicate the positions of the fixed probes.

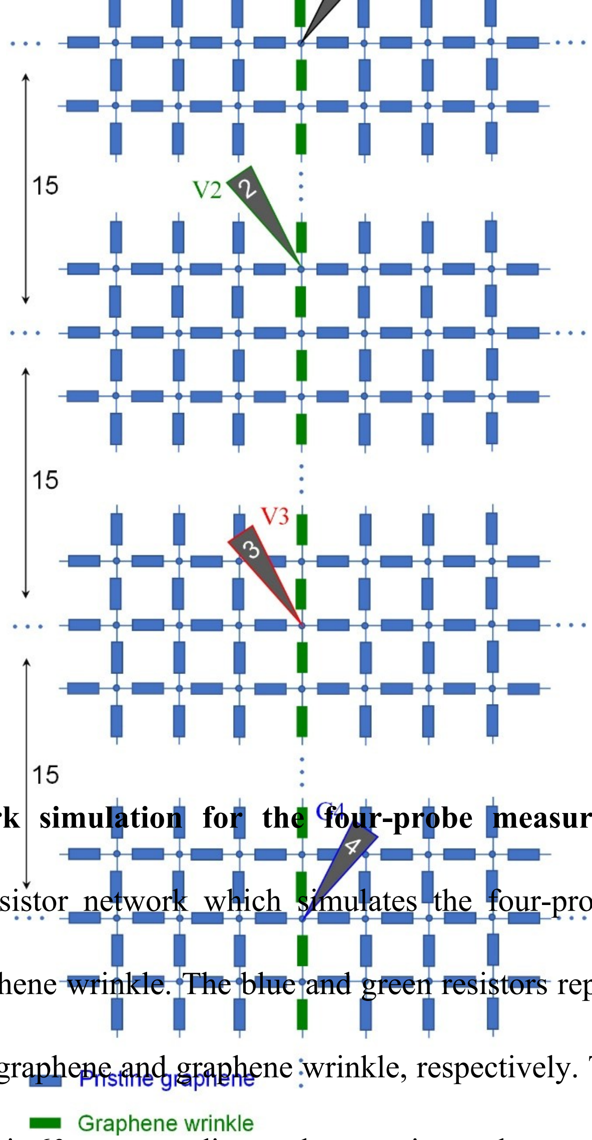

Fig. S3. Resistor network simulation for the four-probe measurements. (a) Schematics of 75 × 75 resistor network which simulates the four-probe collinear measurements along a graphene wrinkle. The blue and green resistors represent 4 μm × 4 μm area in the pristine graphene and graphene wrinkle, respectively. The distance between two nearest probes is 60 μm according to the experimental setups.

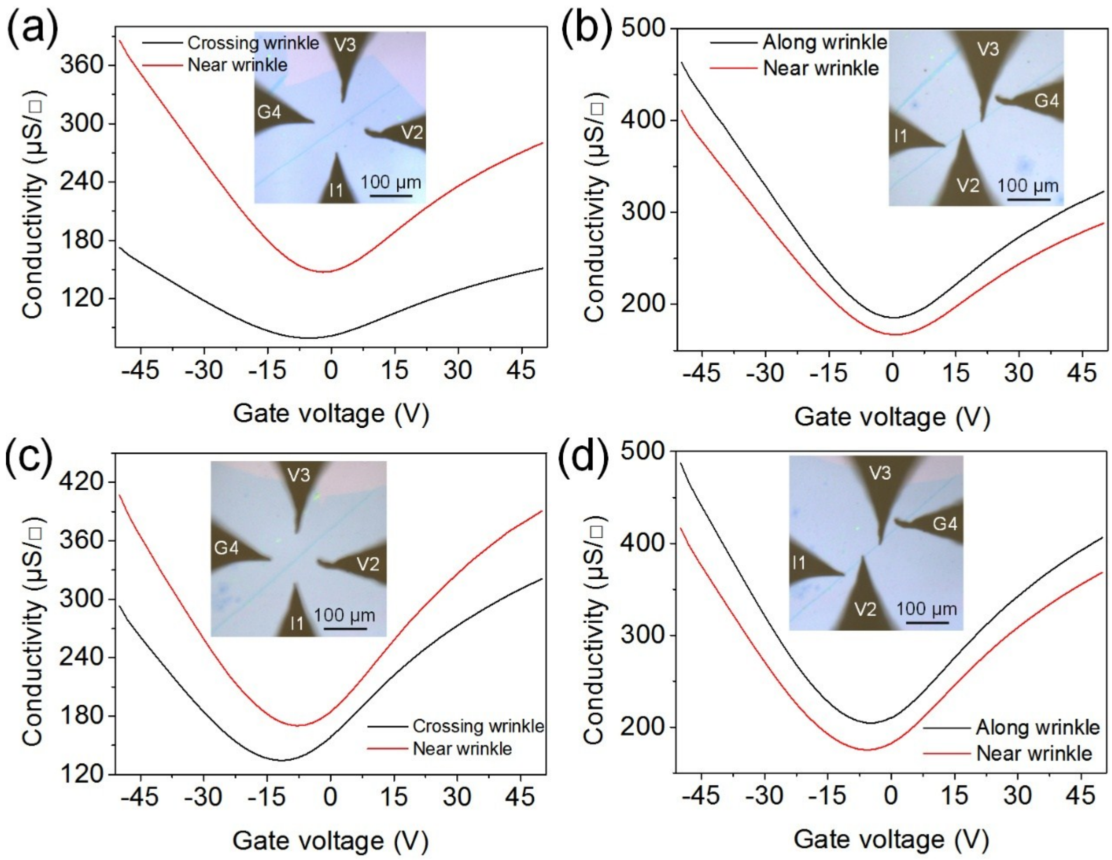

Fig. S4. Four-probe measurement of gate-tunable conductivity on CVD-grown graphene. (a-b) Gate-tunable conductivity of graphene wrinkle-2 in four-probe square and collinear configurations, respectively. The inset shows the optical micrographs during the four-probe measurements. (c-d) The results from graphene wrinkle-3 by the same method as wrinkle-2. The conductivity across the graphene wrinkle is much lower than the case on monolayer area while the conductivity along the graphene wrinkle is higher than that in the monolayer region.

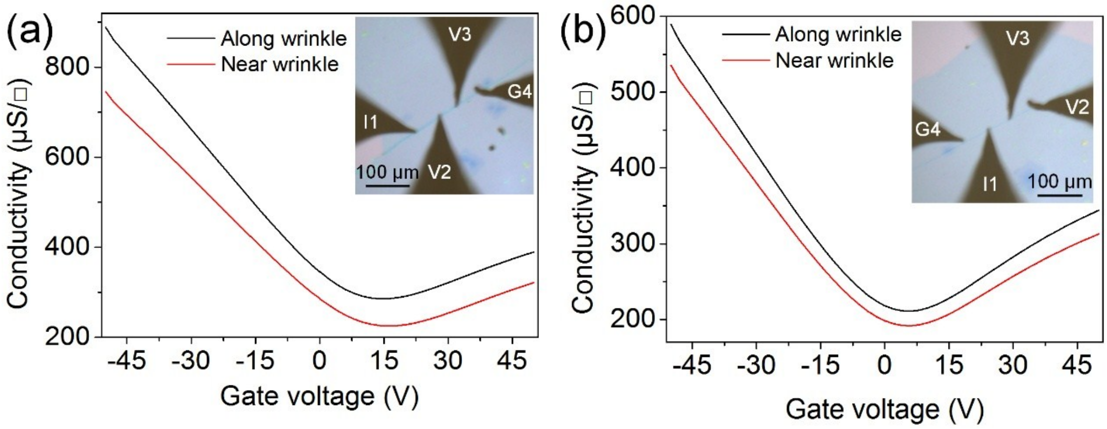

Fig. S5. Four-probe collinear measurement of gate-tunable conductivity along and near the graphene wrinkles. (a) Gate-tunable conductivities of graphene wrinkle-4 in four-probe collinear configuration. The inset show the optical micrographs during the four-probe electrical measurements. (b) The conductivity results from graphene wrinkle-5 by the same method as (a). The conductivities along the graphene wrinkle are higher than that in the monolayer region near the wrinkle.

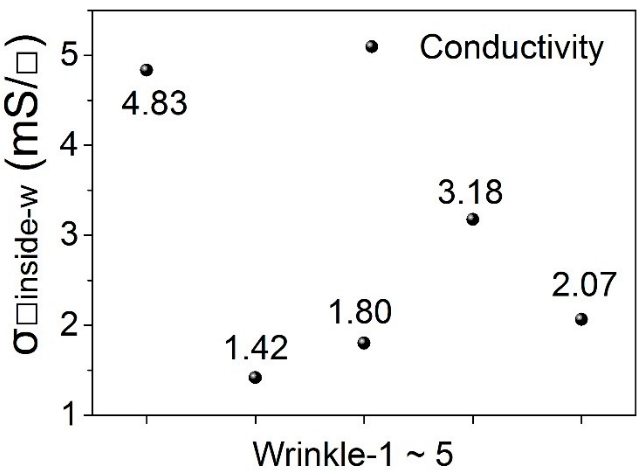

Fig. S6. Conductivity of five graphene wrinkles at charge neutral point in this paper. The conductivity solely in the wrinkled region are on the order of several mS/□

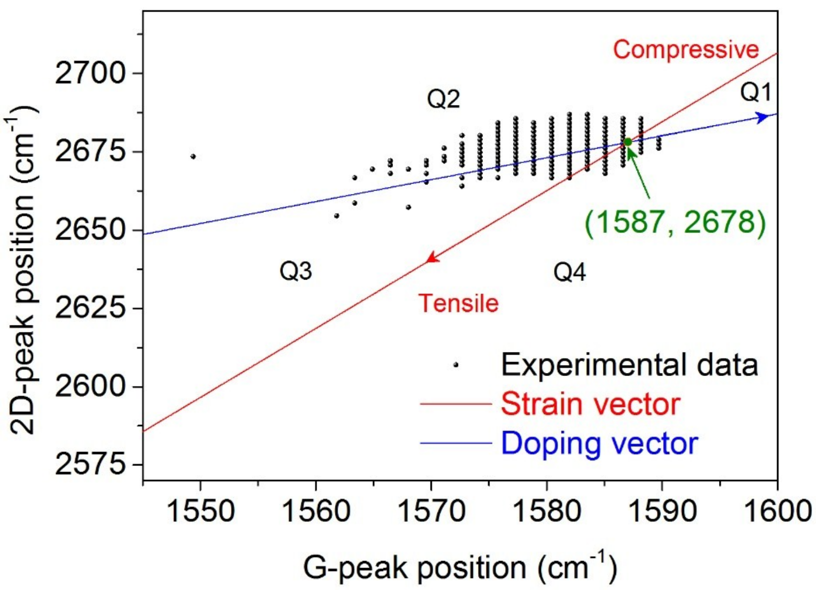

Fig. S7. Correlation between the Raman shift of the G and 2D peaks of graphene area with wrinkle on SiO_2/Si substrate. The strain and doping vector lines intersect at (1587, 2678), which are averaged reference values for the flat monolayer region far away from the wrinkled area in this paper.

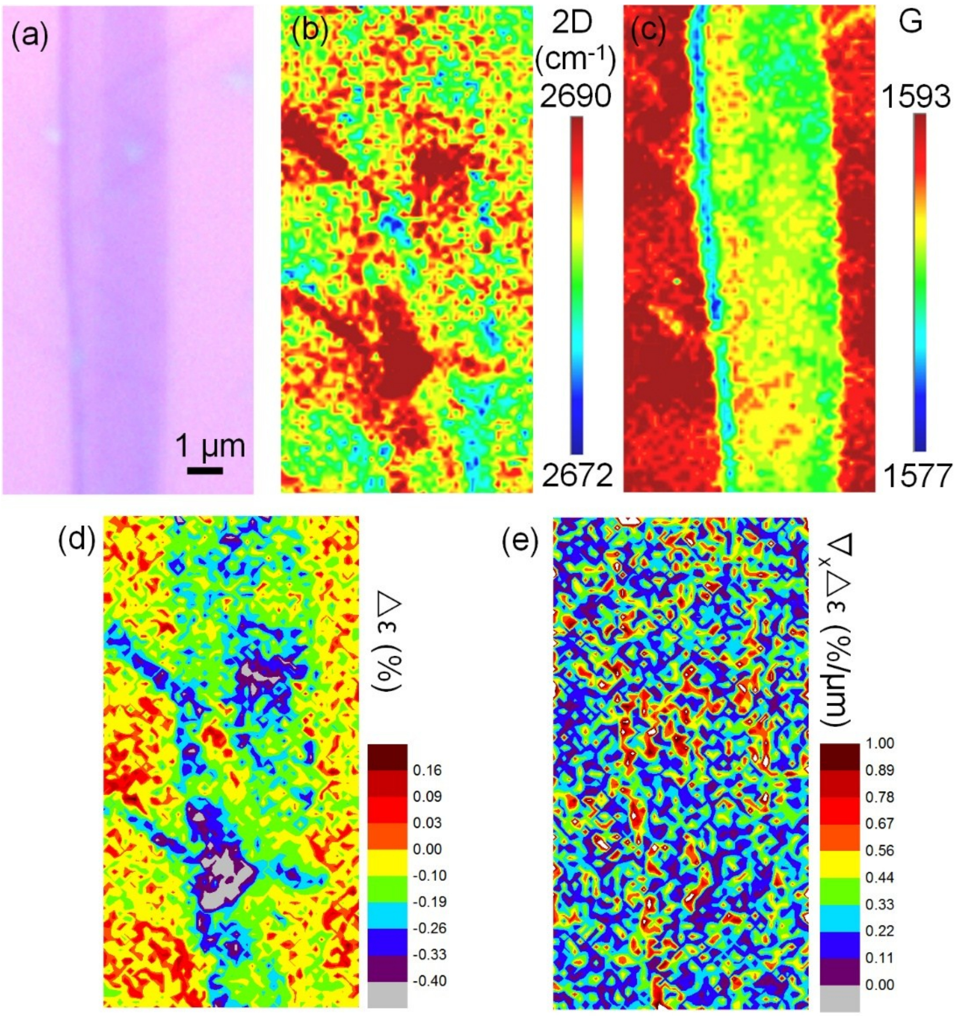

Fig. S8. Raman characterization of the wrinkle-2 area. (a) Optical image of the characterized graphene wrinkle-2. (b-c) Raman mapping of 2D and G peak positions of the graphene wrinkle-2 shown in (a). (d) Contour map for strain distribution extracted from Raman 2D and G mapping shown in (b-c). The wrinkled areas show compressive strain up to 0.54% while the monolayer regions near the wrinkle show tensile strain up to 0.18%. (e) Mapping of strain gradients along the perpendicular direction relative to the wrinkle.

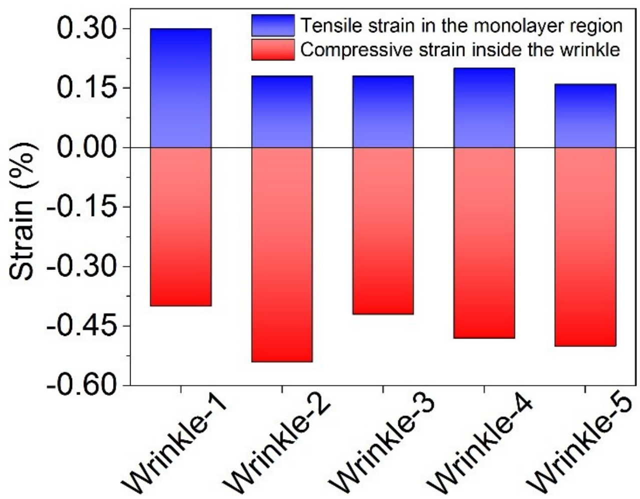

Fig. S9. Strain variations of the wrinkled regions and monolayer regions near the wrinkle for the five wrinkles in this paper. The wrinkled regions show compressive strain up to ~0.5% while the monolayer regions near the wrinkle present tensile strain up to ~0.3%.